

## Metal hydride hydrogen sensing materials from 28 °C to 270 °C

Dewi, H.; Dissanayake, K. P.; Schreuders, H.; Groves, R. M.; Bannenberg, L. J.

**DOI**

[10.1016/j.ijhydene.2024.08.128](https://doi.org/10.1016/j.ijhydene.2024.08.128)

**Publication date**

2024

**Document Version**

Final published version

**Published in**

International Journal of Hydrogen Energy

**Citation (APA)**

Dewi, H., Dissanayake, K. P., Schreuders, H., Groves, R. M., & Bannenberg, L. J. (2024). Metal hydride hydrogen sensing materials from 28 °C to 270 °C. *International Journal of Hydrogen Energy*, *84*, 606-614. <https://doi.org/10.1016/j.ijhydene.2024.08.128>

**Important note**

To cite this publication, please use the final published version (if applicable). Please check the document version above.

**Copyright**

Other than for strictly personal use, it is not permitted to download, forward or distribute the text or part of it, without the consent of the author(s) and/or copyright holder(s), unless the work is under an open content license such as Creative Commons.

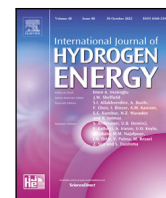
**Takedown policy**

Please contact us and provide details if you believe this document breaches copyrights. We will remove access to the work immediately and investigate your claim.



Contents lists available at ScienceDirect

## International Journal of Hydrogen Energy

journal homepage: [www.elsevier.com/locate/he](http://www.elsevier.com/locate/he)

## Metal hydride hydrogen sensing materials from 28 °C to 270 °C

H.S. Dewi<sup>a,b,\*</sup>, K.P. Dissanayake<sup>a</sup>, H. Schreuders<sup>b</sup>, R.M. Groves<sup>a</sup>, L.J. Bannenberg<sup>b</sup><sup>a</sup> Department of Aerospace Structures and Materials, Delft University of Technology, Kluyverweg 1, Delft, 2629 HS, The Netherlands<sup>b</sup> Faculty of Applied Sciences, Delft University of Technology, Van der Maasweg 9, Delft, 2629 HZ, The Netherlands

## ARTICLE INFO

## Keywords:

Palladium

Tantalum

Optical sensors

Thin films

Optical transmission

Thermal expansion

## ABSTRACT

Metal hydrides have been widely studied as hydrogen sensing materials and applied to various optical sensor configurations. With the increasing interest in using hydrogen as an energy source across sectors involving combustion processes, there is a growing demand for reliable hydrogen sensors operating at temperatures above 100 °C. Therefore, it is necessary to evaluate the performance of potential hydrogen sensing materials at elevated temperatures. We conducted experiments to observe the optical response and structural characteristics of palladium, palladium–gold, tantalum, and tantalum–alloy thin films with respect to varying hydrogen concentrations from 28 °C to 270 °C. Our results demonstrate that the optical response of palladium and palladium–gold diminish at 270 °C. However, tantalum provides a remarkable optical response to hydrogen concentrations below 1% for all the observed temperatures and a stable response at 270 °C for 350 cycles. Our measurement results show that tantalum is the most suitable material for detecting hydrogen within the range of 0.01% to 100% at temperatures ranging from 28 °C to 270 °C.

## 1. Introduction

Hydrogen has a high energy density per mass and produces water vapour as its primary combustion product [1–3]. Such high energy density per mass makes hydrogen an appealing energy source in various sectors including aerospace, metallurgy, automotives, and chemical industries [4–7]. The high energy density of hydrogen can reduce the fuel weight on vehicles and aircrafts, creating a more efficient propulsion system compared to conventional fuels. In the steel-making process, the use of hydrogen can significantly improve process efficiency while reducing carbon emissions [7,8]. These applications of hydrogen involve high temperatures above 100 °C. Since hydrogen is highly explosive and high temperatures increase the risk of explosions, it is crucial to monitor the hydrogen concentration in the surrounding areas as safety precautions. Therefore, there is a need to develop hydrogen sensor which can operate from the room temperature to beyond 100 °C.

Optical sensors can be small in size, lightweight, immune to electromagnetic interference and sparks and have remote sensing capability [9]. These sensors can be modified and adapted into hydrogen sensors by integrating a hydrogen reactive material that can change its optical properties with respect to varying hydrogen concentrations [10–13]. For instance, metal hydride thin films are known to change their optical properties upon contact with hydrogen due to absorption of hydrogen, which depends on the pressure of hydrogen and temperature according to Van't Hoff's law [14–17].

Palladium and palladium alloy are by far the most studied hydrogen sensing materials [18–21]. Hydrogen molecule dissociation can occur effortlessly on their surface due to their low activation energy. After dissociation, the hydrogen atoms diffuse into the material and occupy interstitial sites of the lattice. At sufficiently high hydrogen pressure, a first order phase transformation occurs between a low-hydrogen content  $\alpha$ -phase PdH<sub>x</sub> to the high-hydrogen content  $\beta$ -phase PdH<sub>x</sub> which is accompanied by a significant lattice expansion. This phase transition can provide prominent optical contrast in a narrow pressure range. The first order phase transition implies hysteretic behaviour which can cause an ambiguous optical response that limits the sensing accuracy, while the narrow pressure range indicates narrow sensing range. As such, palladium has often been alloyed with elements. For instance, gold reduces the hysteretic behaviour and broadens the sensing range at the expense of a reduced optical contrast [21–25].

Recently, tantalum has emerged as an attractive hydrogen sensing material due to its hysteresis free optical response at a wide sensing range, particularly at low hydrogen pressures [26]. Hydrogen absorption in tantalum causes gradual changes in optical properties and lattice expansion without a first order phase transformation [27]. This characteristic of tantalum promises reversible optical response with respect to changing hydrogen concentrations. Additionally, the sensing range can be tuned by varying alloying elements and/or compositions that promotes high adaptability to various applications [26,28].

\* Corresponding author at: Department of Aerospace Structures and Materials, Delft University of Technology, Kluyverweg 1, Delft, 2629 HS, The Netherlands.  
E-mail address: [h.s.dewi@tudelft.nl](mailto:h.s.dewi@tudelft.nl) (H.S. Dewi).

<https://doi.org/10.1016/j.ijhydene.2024.08.128>

Received 7 June 2024; Received in revised form 5 August 2024; Accepted 7 August 2024

Available online 21 August 2024

0360-3199/© 2024 The Authors. Published by Elsevier Ltd on behalf of Hydrogen Energy Publications LLC. This is an open access article under the CC BY license (<http://creativecommons.org/licenses/by/4.0/>).

Both palladium and tantalum have been studied at room temperature up to around 100 °C. Following the need of hydrogen sensors at temperatures above 100 °C, studies on the sensing functionality of these materials at elevated temperature are required.

Operating temperatures above 100 °C pose challenges for the sensing materials. First, the detection limit can fall above the explosive limit of hydrogen due to shift of the sensing range following Van't Hoff's law. Accordingly, measurements of the optical response at temperatures above 100 °C are needed to identify the shift of the sensing range and thus detection limit of the sensing materials at high temperatures.

Second, interdiffusion of the thin film layers may occur due to prolonged exposure to high temperatures. The hydrogen sensing material usually consists of two or more thin film layers. For example, the tantalum system consists of an adhesive layer made from titanium, the tantalum sensing layer, and a catalytic layer of palladium–gold. Previous studies on Ti–Au–Pd and Pd–Au films reported that interdiffusion occurred after annealing from 200 °C to 490 °C [29,30]. Structural damages, such as delamination and cracks, were also reported on palladium thin films after hydrogen absorption at room temperature [31,32]. These suggest that structural analysis at temperatures above 100 °C is valuable for examining the tolerance and life-time of the sensing materials.

This study aims to identify the sensing performance of palladium- and tantalum-based thin films at temperatures above 100 °C. We measured the optical response of palladium, palladium–gold and tantalum-alloy thin films in respect to changing hydrogen pressures from 28 °C to 270 °C. These optical measurements identify the sensing range of the materials for variety of working temperatures. The tolerance of the thin films to high temperatures was investigated using X-ray diffraction and reflectometry analysis, including continuous exposure to 350 cycles of changing hydrogen concentrations at 270 °C.

## 2. Methodology

The following subsections describe the details of materials characterisations and the fabrication of specimens.

### 2.1. Fabrication of specimens

The specimens are layers of metal thin film on fused quartz substrates ( $10 \times 10 \times 0.5 \text{ mm}^3$ ) as illustrated in Fig. 1(a), consisting of adhesive layer (4 nm titanium) and a hydrogen sensing layer (40 nm of Pd, Pd<sub>1-x</sub>Au<sub>x</sub>, or Ta<sub>1-x</sub>Ru<sub>x</sub>, or Ta<sub>1-x</sub>Pd<sub>x</sub>). The 40 nm thickness of the hydrogen sensing layer was chosen to maintain consistency with our previous studies [26,28]. A catalyst layer (10 nm of Pd<sub>0.6</sub>Au<sub>0.4</sub>) was added on Ta, Ta<sub>1-x</sub>Ru<sub>x</sub>, and Ta<sub>1-x</sub>Pd<sub>x</sub> specimens to accelerate the hydrogenation kinetics and prevent oxidation of the metal hydride [33]. We deposited the thin films using magnetron sputtering in an ultrahigh vacuum chamber (AJA Int.) with a base pressure of  $10^{-6}$  Pa. The deposition occurred under 0.3 Pa of Ar and the substrates were rotated during the deposition to enhance the homogeneity of the layers. The sputtering parameters and conditions are the same as our previous works [24,26,28]. For Pd<sub>1-x</sub>Au<sub>x</sub>, Ta<sub>1-x</sub>Ru<sub>x</sub>, and Ta<sub>1-x</sub>Pd<sub>x</sub> thin films, we sputtered two targets at the same time and adjusted the DC supply to achieve the desired compositions. The targets have a diameter of 50.8 mm and a purity of 99.9%.

### 2.2. Optical properties as a function of hydrogen concentration

We measured changes in optical transmission values of the thin films upon exposure to a variety of hydrogen partial pressures using the hydrogenography set-up [34]. The hydrogenography set-up consists of a pressure chamber which can accommodate up to 9 samples, an oven to control the temperature of the pressure chamber, an illumination source, a camera, and a PC connected to a pressure controller. Both the pressure chamber and the oven have optical windows at the top and

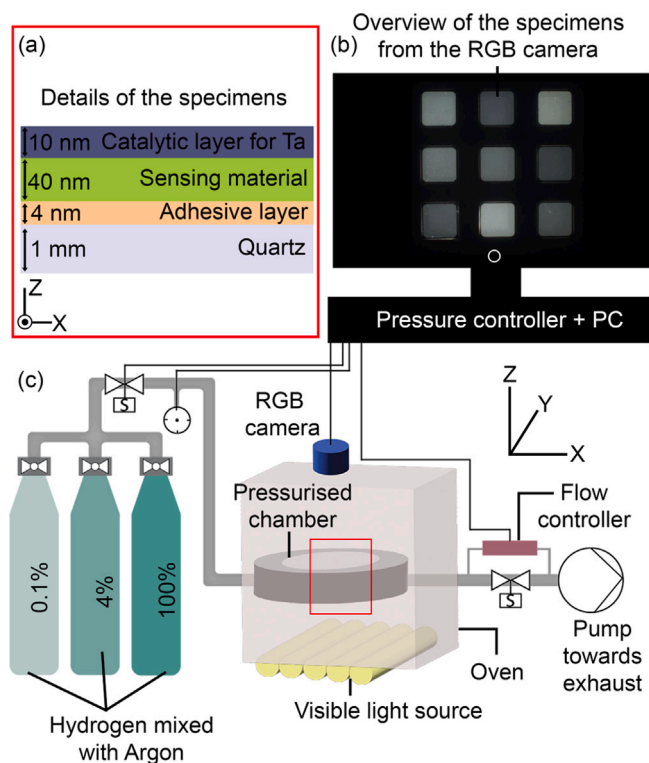


Fig. 1. Illustration of the hydrogenography set-up measuring changes in the transmission of metal thin films upon contact with hydrogen, including (a) schematic of the thin film stack on quartz substrates, (b) overview of the specimens during exposure to hydrogen gas seen from the camera, and (c) gas flow towards the pressurised chamber where the specimens were located. For interpretation of the colour references in this figure legend, please refer to the web version of this article.

bottom that allow transmission of illumination to the camera. Fig. 1(c) depicts the schematic of hydrogenography set-up.

Variation of hydrogen partial pressure ( $P_{H_2}$ ) was achieved by changing the absolute concentrations of hydrogen in argon gas following

$$P_{H_2} = P \times C \quad (1)$$

where  $P$  corresponds to the pressure of the pressured chamber and  $C$  is the relative concentration of hydrogen in argon in which we used variation of 0.1%, 4%, and 100%. A Labview program running on a PC controls and records the gas pressure and flow during the measurements. We programmed increment and decrement steps of pressures (between 0.5 to  $10^6$  Pa) every 15–30 min in the pressure chamber with a typical flow between 10–20 ml/min. These set-points were sent to the flow controller and the pressure controller (MKS Type 250E) which is connected to a solenoidal inlet valve to adjust the pressure in the pressure chamber. A manometer (MKS Baratron) recorded the actual pressure in the pressure chamber ( $P$  in Eq. (1)). We further converted  $P_{H_2}$  to hydrogen concentration in the atmosphere ( $C_{H_2}$ ) using

$$C_{H_2} = \left[ \frac{P_{H_2}}{P_{atm}} \right] \times 100\% \quad (2)$$

where  $P_{atm}$  equals to 101 325 Pa.

Meanwhile, a wide visible light source (five Philips MR16 MASTER LEDs 10/50 W, emission profile is available in Figure S1) illuminated the pressurised chamber from below and the camera (Imaging Source DFK 23UM021 with Aptina CMOS MT9M021, see Figure S1 for quantum efficiency profile) captured the intensity of the transmitted light from the top. Additionally, an IR-filter was mounted before the camera lens to eliminate signals coming from spectrum above 700 nm. Furthermore, considering the measurement range and the difference

in the optical transmission values between the red, green, and blue channels, the green channel with measurement range of 450–700 nm was chosen for this study. An example of the recorded transmission from the specimens is depicted in Fig. 1(b). The bright squares in Fig. 1(b) indicate the specimens where each square corresponds to one type of metal hydride. The PC captured this image every 1 s and this procedure was carried out at 28 °C, 90 °C, 150 °C, 210 °C, and 270 °C.

### 2.2.1. Data processing

To examine the optical transmission of the specimens with changes in hydrogen concentration, we carried out three steps of data processing on the captured images, starting from image processing. First, we defined region of interests (ROI in the size of approximately  $60 \times 60$  pixels) on the square areas (see Fig. 1(b) where each square corresponds to a sensing material).

The second step is obtaining the optical transmission values ( $\ln(\mathcal{T}_{H_2}/\mathcal{T}_0)$ ) of each material as depicted in Eq. (3).

$$\ln(\mathcal{T}_{H_2}/\mathcal{T}_0) = \left[ \ln \left\{ \frac{(t_H - t_{dark})}{(t_0 - t_{dark})} \right\} \right] - \left[ \ln \left\{ \frac{(t_c - t_{dark})}{(t_0 - t_{dark})} \right\} \right] \quad (3)$$

Following the defined regions of interest, we took the mean value of each ROI during hydrogen exposure ( $t_H$ ), without hydrogen exposure ( $t_0$ ) and corrected these values using the dark noise ( $t_{dark}$ ). The ratio of these values was further corrected by a reference sample ( $t_c$ ) that is a material which does not change optical properties with hydrogen (i.e. Al, Ta<sub>50</sub>Pd<sub>50</sub>) to compensate for intensity fluctuations of the light source. We applied this step to all recorded images.

The last step is merging the transmission values and the pressure data. As the material was exposed to a constant hydrogen concentration for 15–30 min, we took an average of the transmission values collected during 10–15 min of hydrogen exposure with camera frame rates of 1 fps. This average transmission value represents the transmission of the specimen at a specific hydrogen partial pressure which becomes the data point of Fig. 3. The three steps of data processing were performed simultaneously in Python.

### 2.3. Stability at high temperature

As the materials change their optical properties upon exposure to hydrogen, the stability test measures the repeatability of these changes. The test is performed by exposing the material to 350 cycles of changing hydrogen concentration in the atmosphere ( $C_{H_2}$  in Eq. (2)) at 270 °C. The observed concentrations are 0.4% and 4% with a baseline of 0.01%. The concentration changes every 5 min between 0.01% – 4% – 0.01% – 0.4% and the experimental set-up was the same as in Section 2.2.

### 2.4. Structural analysis

Exposure to temperatures above room temperature increases the chance of structural damages in the thin films, such as interface mixing or delamination. The structural analysis focuses on examining the integrity of the thin film layers in respect to changing temperature and hydrogen concentrations. We used X-ray reflectometry (XRR) to observe the existence of thin-film layers in the specimens and to measure the thickness of the sensing materials. Additionally, X-ray diffraction (XRD) was performed to evaluate the phases of the thin films and to monitor the  $d$ -spacing (lattice spacing) of the sensing materials upon contact with changing temperatures and hydrogen concentrations. Both measurement techniques were performed using a Bruker D8 Discovery (Cu K $\alpha$ ,  $\lambda = 0.1542$  nm) with a LYNEXE XE detector operating in OD mode and a Göbel mirror. The specimens were placed inside a dome which allows in-situ measurements in respect to changing temperature and gas pressure. Below are the additional details of the measurement procedure.

#### 2.4.1. Structural analysis in respect to temperature

The specimens were heated to 28 °C, 60 °C, 90 °C, 120 °C, 150 °C, 180 °C, 210 °C, and 270 °C and the temperature was kept constant during the measurements. The measurement started 15 min after the set temperatures were reached to ensure equilibrium and the specimens were exposed to surrounding air. The height and angle of the specimens were re-aligned for every temperature to minimise the errors from mispositioning due to thermal expansion. The XRR measurements (0–5°) were carried out using 0.1 mm slits (3 pcs), whereas the Bragg–Brentano XRD was performed with three 0.6 mm slits at angle of  $2\theta = 30$ –90°.

#### 2.4.2. Structural analysis in respect to hydrogen exposure

Measurements related to changing hydrogen partial pressures were performed at a constant temperature of 270 °C. The height and angle of the specimens were aligned before exposing them to hydrogen containing gas. The specimens were then exposed to 4% hydrogen in helium at a variety of pressures (between  $10^3$  to  $10^6$  Pa) to achieve different hydrogen partial pressure values (see Eq. (1)) and thus hydrogen concentrations in the atmosphere (see Eq. (2)). The pressures were kept constant during the measurements that started approximately one minute after the set pressure was reached. The XRR measured 0–4°, while the XRD was performed on 35–45°. Both measurements were carried out using 0.2 mm slits as exit slit, acceptor slit, and receiving slit.

The XRR data analysis was conducted on GenX3 [35] where the data was fit to a model that estimates the layer thicknesses. The XRD data analysis was carried out in Python by fitting the data to a pseudo-Voigt function for Pd, Pd<sub>1-x</sub>Au<sub>x</sub> and two pseudo-Voigt functions for the Ta, Ta<sub>1-x</sub>Ru<sub>x</sub>, Ta<sub>1-x</sub>Pd<sub>x</sub> samples since they have an additional of Pd<sub>0.6</sub>Au<sub>0.4</sub> as a catalyst layer.

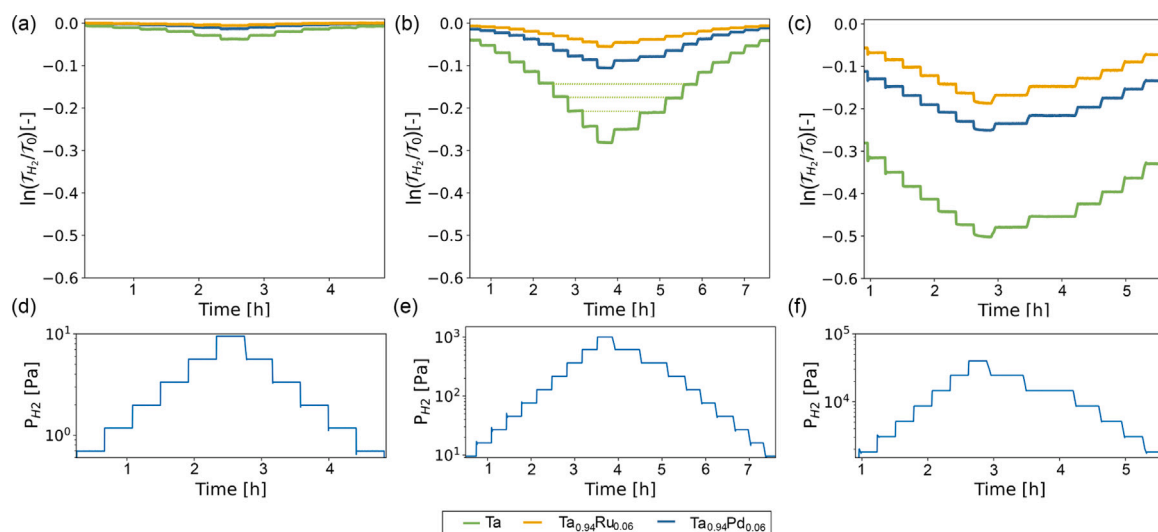
## 3. Results and discussion

A reliable hydrogen sensing material requires several functionalities including (1) being able to provide significant change of optical properties upon small variations of hydrogen pressures, (2) demonstrating reversible and repeatable optical response for multiple cycles of changing hydrogen pressures, (3) providing an optical response across a wide sensing range especially below the explosive limit of hydrogen when it comes to safety purposes, and (4) being able to provide signals at temperatures above 100 °C when heat is involved in the applications. The following passages describe the functionalities of palladium, palladium alloy, tantalum, and tantalum alloy thin films as hydrogen sensing materials when exposed to high temperatures up to 270 °C.

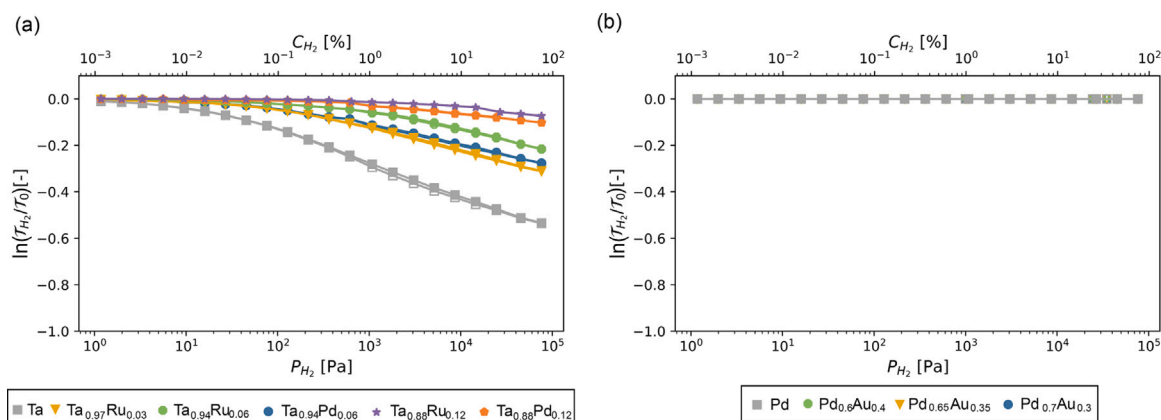
### 3.1. Optical response beyond 28 °C

Fig. 2(a)–(c) depicts the natural logarithm of the relative optical transmission ( $\ln(\mathcal{T}_{H_2}/\mathcal{T}_0)$ ) over time when the hydrogen pressures were varied between  $10^{-2}$  Pa and  $10^5$  Pa at 270 °C, see Fig. 2(d)–(f). The step changes in the optical transmission are well-defined and reflect the changes in hydrogen pressure. Negative  $\ln(\mathcal{T}_{H_2}/\mathcal{T}_0)$  values indicate that the transmission decreases upon exposure to hydrogen and the materials turn more opaque. The  $\ln(\mathcal{T}_{H_2}/\mathcal{T}_0)$  values following the reduced hydrogen partial pressure (dehydrogenation) is the same as when the hydrogen partial pressure increases (hydrogenation; see dashed line on Fig. 2(b)), indicating a reversible effect and the absence of any hysteresis. This result is consistent with the previously reported optical response at room temperature [26,28], implying that the hysteresis free and reversible optical response of tantalum and tantalum alloys continues to occur at 270 °C.

For a better visualisation of the partial hydrogen pressure dependent optical response, we plot  $\ln(\mathcal{T}_{H_2}/\mathcal{T}_0)$  values as a function of hydrogen partial pressures in Fig. 3. It is clear that at 270 °C, the optical response



**Fig. 2.** (a–c) Relative changes of the optical transmission  $\ln(\mathcal{T}_{H_2}/\mathcal{T}_0)$  values of Ta,  $\text{Ta}_{0.94}\text{Ru}_{0.06}$ , and  $\text{Ta}_{0.94}\text{Pd}_{0.06}$  following (d–f) variations of hydrogen partial pressures at 270 °C. Dashed lines in (b) serve as guide to the eye, indicating the same  $\ln(\mathcal{T}_{H_2}/\mathcal{T}_0)$  values after increased and decreased hydrogen partial pressures. Variations of hydrogen partial pressure are (d)  $0.4 \leq P_{H_2} \leq 10$  Pa, (e)  $10 \leq P_{H_2} \leq 1000$  Pa, and (f)  $1000 \leq P_{H_2} \leq 60\,000$  Pa.



**Fig. 3.** Relative changes of optical transmission  $\ln(\mathcal{T}_{H_2}/\mathcal{T}_0)$  values of (a) palladium and (b) tantalum based metal hydrides as a function of hydrogen concentration measured at 270 °C. Each data point corresponds to mean value of the relative transmission at a constant hydrogen partial pressure during increments (filled marks) and decrements (non-filled marks) of the hydrogen partial pressures.

of tantalum and tantalum alloy thin films begins from a very low hydrogen concentration (around  $10^{-3}\%$  –  $10^{-2}\%$ ). The onset of optical response shifts towards high hydrogen concentrations as the amount of alloying composition increases due to compression of the unit cell of the sensing material. Substitution by the alloying elements in tantalum reduces the volume of unit cell, leading to a lower amount of hydrogen absorbed into the materials. The volume compression of the unit cell is also element dependent [28]. For instance, ruthenium causes a larger reduction of unit cell volume compared to palladium at the same concentrations that can be seen in the  $\mathcal{T}_{H_2}/\mathcal{T}_0$  values of  $\text{Ta}_{0.94}\text{Ru}_{0.06}$ ,  $\text{Ta}_{0.94}\text{Pd}_{0.06}$ ,  $\text{Ta}_{0.88}\text{Ru}_{0.12}$ , and  $\text{Ta}_{0.88}\text{Pd}_{0.12}$ .

In comparison to tantalum and tantalum alloy thin films, palladium and palladium–gold thin films provide no optical response towards changing hydrogen concentrations at 270 °C, as presented in Fig. 3(b).

To further investigate the shift of optical response at varying temperatures, we plotted the  $\ln(\mathcal{T}_{H_2}/\mathcal{T}_0)$  values for several temperatures between 28 °C and 270 °C in Fig. 4. The figure demonstrates that the optical response shifts towards higher hydrogen pressures when a higher temperature is applied to the materials. This phenomenon is expected to occur according to the Van't Hoff's law. However, these results suggest that tantalum and tantalum alloy are still able to provide a wide sensing range particularly at low hydrogen pressures (below  $10^3$

Pa or lower than 1% of hydrogen concentration in the atmosphere) even at elevated temperatures up to 270 °C.

Meanwhile, the optical response of palladium and palladium alloy diminishes at elevated temperatures, for example at 150 °C, the detectable optical response begins at a very high hydrogen pressure (above  $10^4$  Pa or more than 10% of hydrogen concentration in the atmosphere). Given that the lower flammability limit of hydrogen in the air is around 4% [36,37], palladium and palladium alloy are not suitable as hydrogen sensing materials for safety purposes at temperatures above 90 °C.

With regards to the application for hydrogen sensors, tantalum and tantalum alloy demonstrate a remarkable optical response from 28 °C to 270 °C. A reversible optical response can be easily achieved due to the absence of hysteresis. Furthermore, the sensing range at high temperatures still covers hydrogen concentrations below 1% and can be further tuned by varying alloying elements or compositions.

### 3.2. Stability of the optical response at 270 °C

In addition to providing a wide sensing range at various temperatures, a reliable sensing material should be able to produce a consistent response over a long period of time with continuously changing hydrogen concentrations. Fig. 5 shows the results of stability tests performed

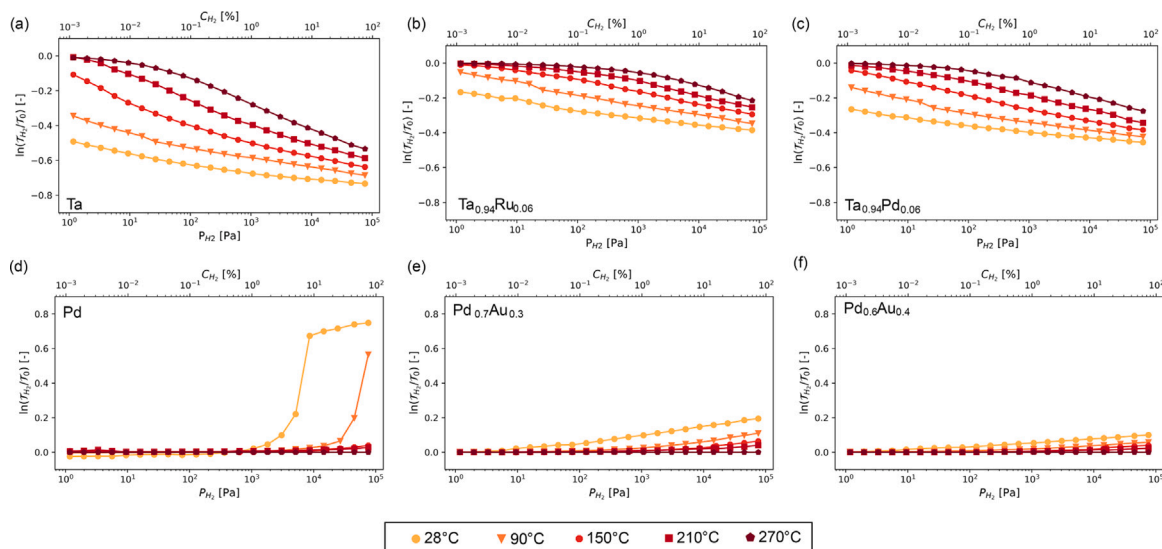


**Fig. 4.** Relative changes of optical transmission  $\ln(\mathcal{T}_{H_2}/\mathcal{T}_0)$  of (a)–(c) tantalum alloy and (d)–(f) palladium alloy as a function of hydrogen concentration measured at various temperatures from 28 °C to 270 °C. The data represents values obtained after stepwise increasing the hydrogen partial pressures.

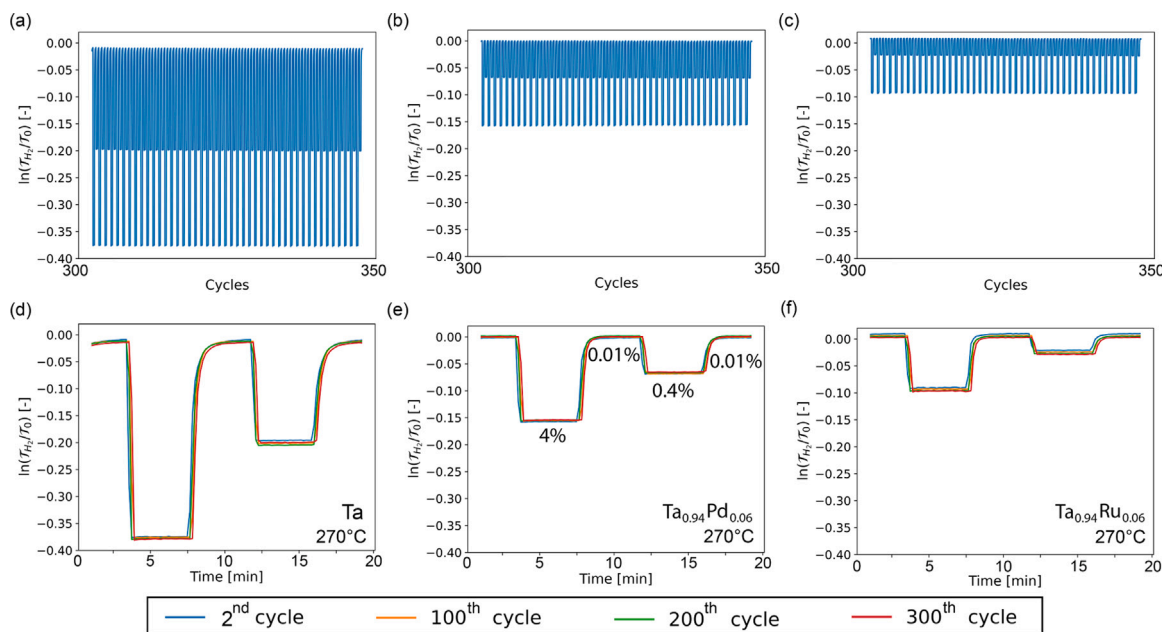


**Fig. 5.** Optical response of Ta, Ta<sub>0.94</sub>Pd<sub>0.06</sub>, and Ta<sub>0.94</sub>Ru<sub>0.06</sub> during 350 cycles of changing hydrogen concentrations at 270 °C.  $\ln(\mathcal{T}_{H_2}/\mathcal{T}_0)$  values corresponding to 50 cycles are depicted in (a)–(c), while details of the optical transmission for every 100 cycles are shown in (d)–(f).

on tantalum, tantalum–palladium, and tantalum–ruthenium specimens where (a)–(c) depict the  $\ln(\mathcal{T}_{H_2}/\mathcal{T}_0)$  values during 50 cycles taken after cycle 300, while (d)–(f) illustrate the  $\ln(\mathcal{T}_{H_2}/\mathcal{T}_0)$  values during one cycle and being compared for every 100 cycles. The graphs demonstrate immediate response and recovery time following the change in hydrogen concentrations.

The stability test results show that the optical response of tantalum and tantalum alloy is stable for at least 300 cycles at 270 °C, indicated by the identical distribution of  $\ln(\mathcal{T}_{H_2}/\mathcal{T}_0)$  values over 350 cycles. This implies that the optical response is highly repeatable, promising accuracy and reliability above room temperatures up to 270 °C.

Fig. 5 shows that the optical contrast of tantalum is the highest among the three materials followed by tantalum–palladium, and tantalum–ruthenium. Optical contrast refers to changes in  $\ln(\mathcal{T}_{H_2}/\mathcal{T}_0)$  values following the change in hydrogen pressures/concentrations which in this case is between 0.01%–0.4%–4%. As a large contrast

can be related to sensitivity, tantalum can potentially provide better sensitivity compared to tantalum–palladium and tantalum–ruthenium at 270 °C.

### 3.3. Thermal expansion of the thin films

Prolonged contact to elevated temperatures can expand the thin films which may cause damages, such as cracks, delamination or inter-diffusion. We measure lattice spacing and layer thickness of the sensing material using XRD and XRR with respect to changing temperatures to examine the thermal expansion of the thin films and possibility of damages in the thin film layers.

Lattice expansion of the thin films is indicated by the shift of the diffraction peak towards lower  $2\theta$  angle. Fig. 6(a) depicts the diffraction pattern of  $\langle 110 \rangle$  Ta<sub>0.94</sub>Ru<sub>0.06</sub> with a capping layer of Pd<sub>0.6</sub>Au<sub>0.4</sub> at 28 °C, 150 °C, and 270 °C. We note that the films are strongly textured

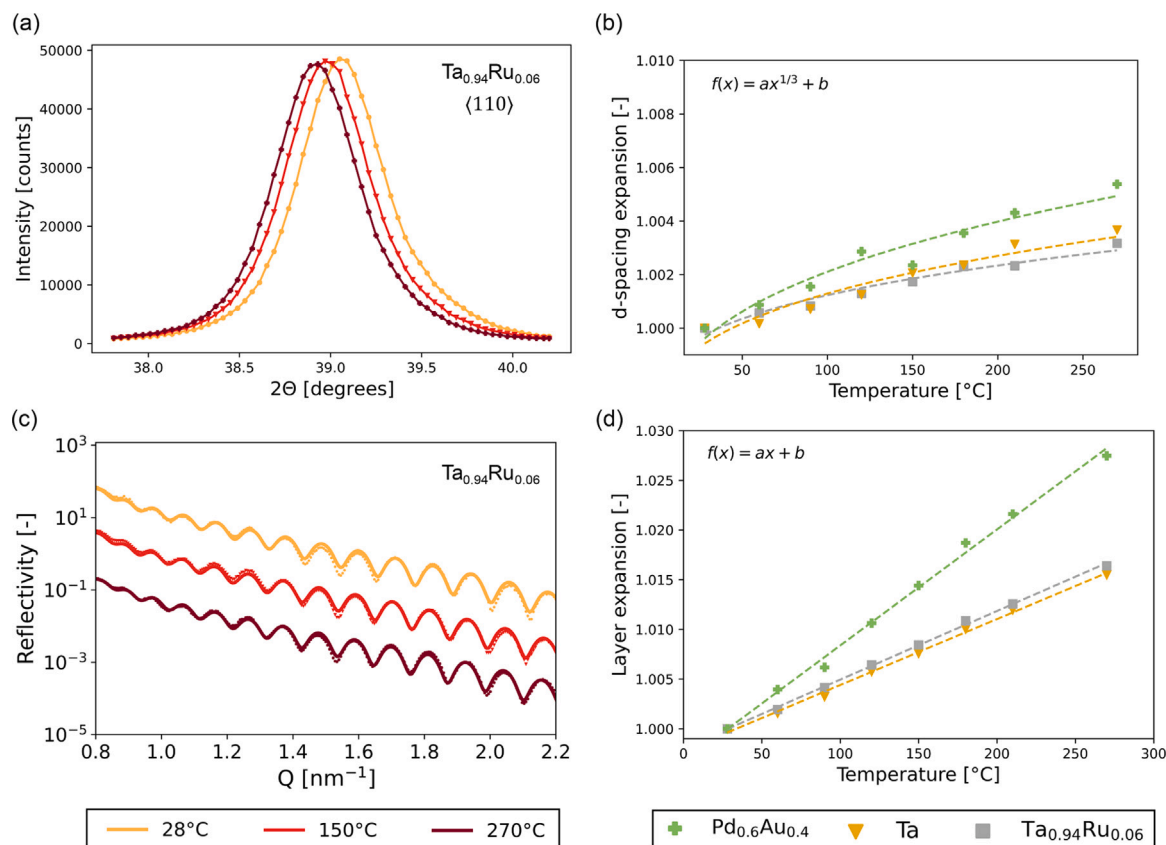


**Fig. 6.** Structural analysis of the thin films consisting of (a) XRD measurements and (b) XRR analysis identifying (c) out-of-plane  $d_{110}$  (Ta, Ta<sub>0.94</sub>Ru<sub>0.06</sub>)/ $d_{111}$  (Pd<sub>0.6</sub>Au<sub>0.4</sub>) and (d) layer expansion due to increase of temperatures. The slopes of the layer expansion correspond to the volumetric thermal expansion of the thin films summarised in Table 1. The dots in (c) indicate the measured data, while the solid lines are the fitting model to the data on the basis of which the layer expansion has been deduced. The corresponding SLD profiles can be found in Figure S6.

**Table 1**

Volumetric thermal expansion coefficient derived from layer expansion in Fig. 6(d) and their comparison to bulk materials [38].

Materials	Measured coefficient ( $10^{-6} \text{ K}^{-1}$ )	Literature ( $10^{-6} \text{ K}^{-1}$ )
Ta	$66.4 \pm 6.56$	19.5
Ta <sub>0.94</sub> Ru <sub>0.06</sub>	$69.07 \pm 3.31$	
Pd <sub>0.6</sub> Au <sub>0.4</sub>	$116.8 \pm 28.62$	42 (Pd alloys)

as only the  $\langle 110 \rangle$  and  $\langle 220 \rangle$  peaks of Ta<sub>0.94</sub>Ru<sub>0.06</sub>, including the  $\langle 111 \rangle$  and  $\langle 222 \rangle$  peaks of Pd<sub>0.6</sub>Au<sub>0.4</sub> were observed in the full diffraction pattern from 30° to 90° (see Figure S4). The diffraction results do not indicate the appearance of an additional phase in the specimens, implying that no phase transition occurs when the thin films are heated up to 270 °C.

The reflectometry results, for which examples are depicted in Fig. 6(c), shows well-defined fringes, indicating the existence of thin film layers in the specimens at temperatures ranging from 28 °C to 270 °C. Given the fact that the specimens were exposed to each temperature for one hour and several days of testing with hydrogen exposure at 270 °C, there is so far no indication of interdiffusion found related to prolonged exposure to high temperatures up to 270 °C. This is consistent with the stability test results.

After obtaining positive results from the diffraction and reflectometry measurements, we calculated the lattice and layer expansion of the sensing materials as summarised in Fig. 6(c) and (d). Since our specimens are thin films, the increase in layer thicknesses corresponds to the increase in volume. It is seen in Fig. 6 that the layer expansion is approximately three times larger than the lattice expansion. Additionally, this also indicates that the thermal expansion is isotropic.

As the volumetric expansion follows a linear trend (see Fig. 6(d)), the slope of a linear fit of the data indicates the volumetric coefficients of thermal expansion. We have summarised these coefficients in Table 1. Compared to the bulk materials, our thin films are about 3 to 4 times higher. It is known that thin films tend to have a distinct thermal expansion coefficient compared to bulk materials due to substrate clamping and surface effects [39]. Therefore, we see a layer expansion three times higher than the lattice expansion and subsequently a larger volumetric thermal expansion coefficient compared to the bulk materials.

#### 3.4. Structural analysis during hydrogen absorption at 270 °C

We have shown that tantalum and tantalum alloy have a remarkable optical response at 270 °C to hydrogen. Finally, this subsection describes their structural behaviour with regards to hydrogen absorption at 270 °C.

In-situ XRD measurements were performed during loading of hydrogen to palladium–gold, tantalum, tantalum–ruthenium, and tantalum–palladium thin films at 270 °C. The diffraction patterns do not indicate any phase transition due to hydrogen absorption as no new additional peaks appear in the patterns. We thus calculated the lattice expansion values as depicted in Fig. 7(a). It is clear that the lattice of palladium–gold does not expand upon exposure to changing hydrogen pressures. This result is aligned to the optical measurements of palladium–gold that does not indicate any optical response at 270 °C.

Then, we compared the out-of-plane lattice expansion with respect to hydrogen exposure measured at 270 °C to the expansion at 28 °C (see Fig. 7(b)) in which the expansion of tantalum and tantalum alloy was reproduced from the literature [26,28]. The figures show that lattice

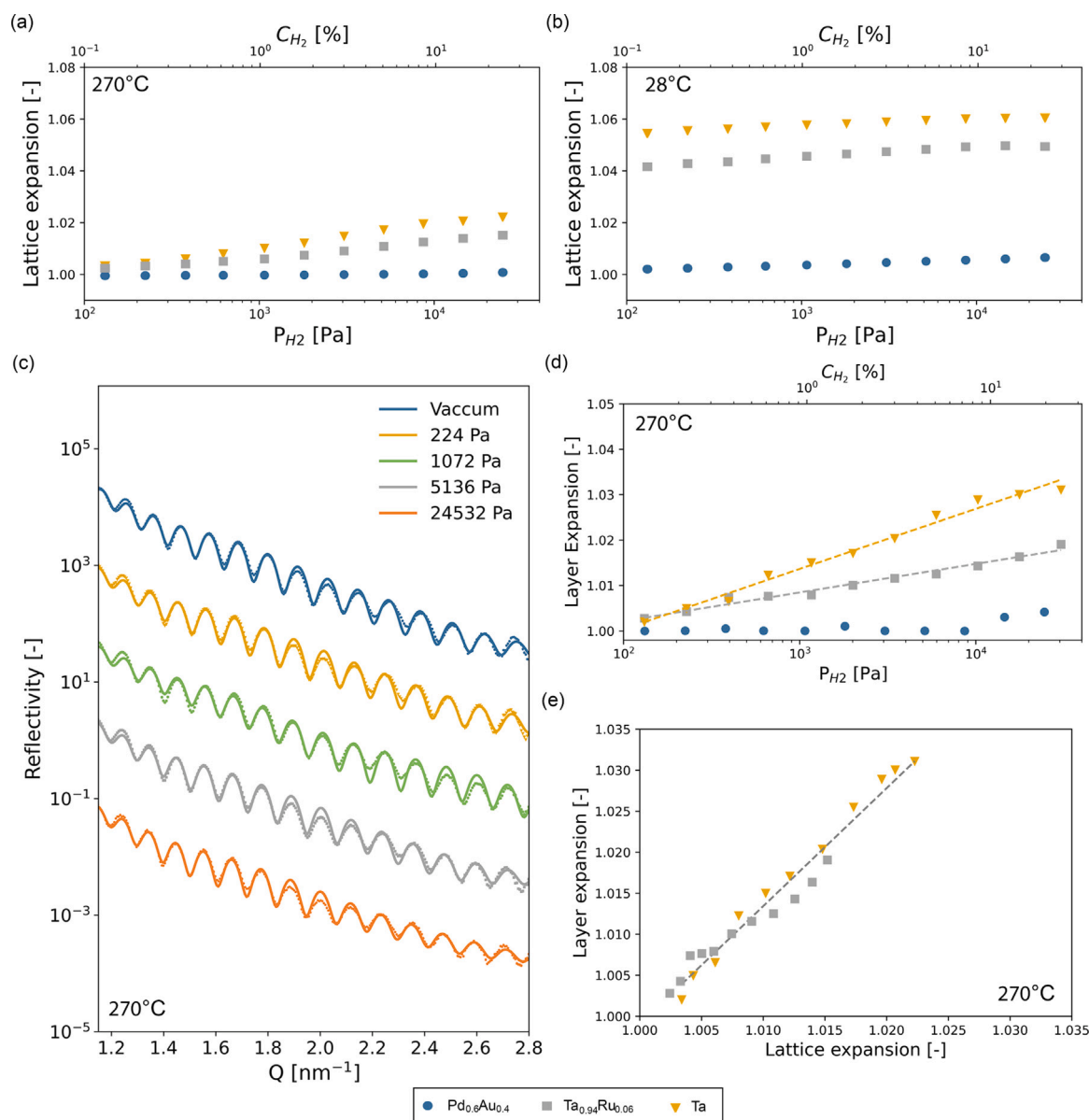


**Fig. 7.** Structural analysis related to hydrogen exposure at 270 °C. (a) and (b) depict a comparison of  $d_{111}/d_{110}$  lattice expansion as a function of hydrogen partial pressure measured at 270 °C and 28 °C. X-ray diffraction patterns measured at 270 °C are available in Figure S5. (c) is an example of an XRR measurement result for  $\text{Ta}_{0.94}\text{Ru}_{0.06}$ . The dots indicate the measured data and the solid lines correspond to the fitted model to the data. The corresponding SLD profiles are available in Figure S6. (d) shows layer expansion derived from the reflectograms, while (e) illustrates the relation of layer and lattice expansion. Lattice expansion of tantalum and tantalum alloy at 28° was reproduced from [26,28].

expansion of tantalum and tantalum alloy is substantially smaller at 270 °C. This is in agreement with Van't Hoff's law and the optical transmission measurements.

The in-situ XRR results at 270 °C, example shown in Fig. 7(c), demonstrate well defined fringes for all the observed hydrogen pressures. This indicates well defined thin film layers with minimum possibility of damages. This result agrees with the stability test and that the thin films are able to produce a stable optical response at 270 °C.

A linear relationship between layer expansion and hydrogen partial pressure was observed for tantalum and tantalum alloy thin films at 270 °C (see Fig. 7(d)). Whereas, palladium–gold thin film does not indicate any changes in the thickness related to hydrogen absorption, which is in accordance to their optical and in-situ XRD measurement results.

To further understand the structural response of the thin films to hydrogen, we plotted the layer expansion of tantalum and tantalum alloy as a function of their lattice expansion in Fig. 7(e). Unlike the thermal expansion, the layer expansion shows a linear relation to the

lattice expansion. This implies that the volumetric expansion due to hydrogen absorption occurs in one direction towards the out-of-plane axis by a gradual elastic deformation of the unit cell. This phenomenon has previously been observed at room temperature as a unique characteristic of tantalum thin film [27]. Hence, this result confirms that the phenomenon still occurs at 270 °C.

The structural behaviour of the thin films is consistent with the optical response described in Section 3.1. Hydrogen absorption followed by elastic deformation of the unit cell occurs at 270 °C which explains the observed optical response of tantalum and tantalum alloy. These results demonstrate that tantalum and tantalum alloy can serve as reliable hydrogen sensing materials at high temperatures up to 270 °C.

#### 4. Conclusions

We have measured the optical response and structural behaviour of palladium, palladium–gold, tantalum, and tantalum alloy thin films upon exposure to varying hydrogen concentrations at 270 °C. The thin

films were exposed to high temperature up to 270 °C and 350 cycles of changing hydrogen concentrations to investigate their durability and stability. These examinations suggest the following findings related to hydrogen sensing at high temperatures.

- Palladium and palladium–gold thin films are able to detect hydrogen below its explosive limit (4%) up to about 90 °C. Beyond this temperature, the detection limit falls above the explosive limit of hydrogen and no optical response can be distinguished at 270 °C.
- Tantalum provides good hydrogen sensing capability up to 270 °C as indicated by a large optical contrast in the range of 0.01% – 100% at temperatures ranging from 28 °C to 270 °C.
- No indications of layer interdiffusions or deformations were found in the thin films due to hydrogen absorption at 270 °C.
- The thin films demonstrate a high tolerance for prolonged exposure to elevated temperatures up to 270 °C. This is shown by the absence of additional peaks in the X-ray diffraction patterns and the persistence of well defined fringes from the XRR measurements.
- Isotropic thermal expansion occurs in the thin film when it is heated up to 270 °C. Volumetric thermal expansion coefficients of the thin films are 3 to 4 times higher than that of bulk materials.
- The expansion resulting from hydrogen absorption at 270 °C takes place along the out-of-plane axis, as indicated by the linear relation between the expansion of the sensing layers and lattice in the thin films.

These findings can be used to design optical hydrogen sensors operating above the room temperature. The thin films can be easily integrated into various optical sensor configurations, such as a (tilted) fibre Bragg grating.

#### CRediT authorship contribution statement

**H.S. Dewi:** Writing – review & editing, Writing – original draft, Investigation, Formal analysis, Data curation, Conceptualization. **K.P. Dissanayake:** Writing – review & editing, Investigation, Formal analysis. **H. Schreuders:** Writing – review & editing, Methodology, Formal analysis, Data curation. **R.M. Groves:** Writing – review & editing, Supervision. **L.J. Bannenberg:** Writing – review & editing, Supervision, Methodology, Formal analysis.

#### Declaration of competing interest

The authors declare that they have no known competing financial interests or personal relationships that could have appeared to influence the work reported in this paper.

#### Acknowledgements

Authors acknowledge funding from the European Union Clean Aviation programme for the project HYDEA with the project number 101102019 and Horizon programme for the project OVERLEAF with the project number 101056818.

#### Appendix A. Supplementary data

Supplementary material related to this article can be found online at <https://doi.org/10.1016/j.ijhydene.2024.08.128>.

#### References

- [1] Hauglustaine D, Paulot F, Collins W, Derwent R, Sand M, Boucher O. Climate benefit of a future hydrogen economy. *Nat Commun Earth Environ* 2022;3:295. <https://dx.doi.org/10.1038/s43247-022-00626-z>.
- [2] Habib MA, Abdulrahman GA, Alquaity AB, Qasem NA. Hydrogen combustion, production, and applications: A review. *Alex Eng J* 2024;100:182–207. <https://dx.doi.org/10.1016/j.aej.2024.05.030>, URL <https://www.sciencedirect.com/science/article/pii/S1110016824005003>.
- [3] Cipriani G, Di Dio V, Genduso F, La Cascia D, Liga R, Miceli R, Ricco Galluzzo G. Perspective on hydrogen energy carrier and its automotive applications. *Int J Hydrog Energy* 2014;39(16):8482–94. <https://dx.doi.org/10.1016/j.ijhydene.2014.03.174>, URL <https://www.sciencedirect.com/science/article/pii/S0360319914008660>.
- [4] Okolie JA, Patra BR, Mukherjee A, Nanda S, Dalai AK, Kozinski JA. Futuristic applications of hydrogen in energy, biorefining, aerospace, pharmaceuticals and metallurgy. *Int J Hydrog Energy* 2021;46(13):8885–905. <https://dx.doi.org/10.1016/j.ijhydene.2021.01.014>.
- [5] Bilik J, Pustejovska P, Brozova S, Jursova S. Efficiency of hydrogen utilization in reduction processes in ferrous metallurgy. *Sci Iran* 2013;20(2):337–42. <https://dx.doi.org/10.1016/j.scient.2012.12.028>.
- [6] Adler EJ, Martins JR. Hydrogen-powered aircraft: Fundamental concepts, key technologies, and environmental impacts. *Prog Aerosp Sci* 2023;141:100922. <https://dx.doi.org/10.1016/j.paerosci.2023.100922>, Special Issue on Green Aviation.
- [7] Elsheikh H, Evely V. Renewable hydrogen based direct iron ore reduction and steel making with grid assistance. *Energy Convers Manage* 2023;297:117544. <https://dx.doi.org/10.1016/j.enconman.2023.117544>.
- [8] Vogl V, Åhman M, Nilsson LJ. Assessment of hydrogen direct reduction for fossil-free steelmaking. *J Clean Prod* 2018;203:736–45. <https://dx.doi.org/10.1016/j.jclepro.2018.08.279>.
- [9] Jackson DA, Jones JDC. Fibre optic sensors. *Opt Acta: Int J Opt* 1986;33:1469–503. <https://dx.doi.org/10.1080/713821914>, doi: 10.1080/713821914.
- [10] Butler MA, Ginley DS. Hydrogen sensing with palladium-coated optical fibers. *J Appl Phys* 1988;64(7):3706–12. <https://dx.doi.org/10.1063/1.341414>, arXiv:[https://pubs.aip.org/aip/jap/article-pdf/64/7/3706/18619648/3706\\_1\\_online.pdf](https://pubs.aip.org/aip/jap/article-pdf/64/7/3706/18619648/3706_1_online.pdf).
- [11] Ping X, Cao X, Cao C, Lei H, Yang C, Cheng Q, Zhou T, Liu M. Fiber grating hydrogen sensor: Progress, challenge and prospect. *Adv Sensors Res* 2023. <https://dx.doi.org/10.1002/adrs.202300088>.
- [12] Cao R, Wu J, Liang G, Ohodnicki PR, Chen KP. Functionalized PdAu alloy on nanocoons fabricated on optical fibers for hydrogen sensing. *IEEE Sens J* 2020;20:1922–7. <https://dx.doi.org/10.1109/JSEN.2019.2950505>.
- [13] Fisser M, Badcock RA, Teal PD, Janssens S, Hunze A. Palladium-based hydrogen sensors using fiber Bragg gratings. *J Lightwave Technol* 2018;36:850–6. <https://dx.doi.org/10.1109/JLT.2017.2713038>.
- [14] Huiberts JN, Griessen R, Rector JH, Wijngaarden RJ, Dekker JP, de Groot DG, Koeman NJ. Yttrium and lanthanum hydride films with switchable optical properties. *Nature* 1996;380(6571):231–4. <https://dx.doi.org/10.1038/380231a0>.
- [15] Bhuiya MMH, Kumar A, Kim KJ. Metal hydrides in engineering systems, processes, and devices: A review of non-storage applications. 2015. <https://dx.doi.org/10.1016/j.ijhydene.2014.12.009>.
- [16] Chen K, Yuan D, Zhao Y. Review of optical hydrogen sensors based on metal hydrides: Recent developments and challenges. 2021. <https://dx.doi.org/10.1016/j.optlastec.2020.106808>.
- [17] Franke F, Kazula S, Enghardt L. Review and evaluation of metal-hydride-based hydrogen sensors as safety devices for future sustainable aviation, vol. 2454, Institute of Physics; 2023. <https://dx.doi.org/10.1088/1742-6596/2454/1/012001>.
- [18] Chadwick B, Tam-F J, Brungs M, Gal M. A hydrogen sensor based on the optical generation of surface plasmons in a palladium alloy. 1994.
- [19] Langhammer C, Zorić I, Kasemo B, Clemens BM. Hydrogen storage in Pd nanodisks characterized with a novel nanoplasmonic sensing scheme. *Nano Lett* 2007;7:3122–7. <https://dx.doi.org/10.1021/nl071664a>.
- [20] Zhao Z, Carpenter MA, Xia H, Welch D. All-optical hydrogen sensor based on a high alloy content palladium thin film. *Sensors Actuators B* 2006;113:532–8. <https://dx.doi.org/10.1016/j.snb.2005.03.070>.
- [21] Westerwaal RJ, Rooijmans JS, Leclercq L, Gheorghe DG, Radeva T, Mooij L, Mak T, Polak L, Slaman M, Dam B, Rasing T. Nanostructured Pd-Au based fiber optic sensors for probing hydrogen concentrations in gas mixtures. *Int J Hydrog Energy* 2013;38:4201–12. <https://dx.doi.org/10.1016/j.ijhydene.2012.12.146>.
- [22] Wadell C, Nugroho FAA, Lidström E, Iandolo B, Wagner JB, Langhammer C. Hysteresis-free nanoplasmonic Pd-Au alloy hydrogen sensors. *Nano Lett* 2015;15:3563–70. <https://dx.doi.org/10.1021/acs.nanolett.5b01053>.
- [23] Nugroho FAA, Darmadi I, Cusinato L, Susarrey-Arce A, Schreuders H, Bannenberg LJ, da Silva Fanta AB, Kadkhodazadeh S, Wagner JB, Antosiewicz TJ, Hellman A, Zhdanov VP, Dam B, Langhammer C. Metal–polymer hybrid nanomaterials for plasmonic ultrafast hydrogen detection. *Nature Mater* 2019;18(5):489–95. <https://dx.doi.org/10.1038/s41563-019-0325-4>.

- [24] Bannenberg LJ, Nugroho FAA, Schreuders H, Norder B, Trinh TT, Steinke N-J, van Well AA, Langhammer C, Dam B. Direct comparison of PdAu alloy thin films and nanoparticles upon hydrogen exposure. *ACS Appl Mater Interfaces* 2019;11(17):15489–97. <http://dx.doi.org/10.1021/acsami.8b22455>.
- [25] Darmadi I, Nugroho FAA, Langhammer C. High-performance nanostructured palladium-based hydrogen sensors - current limitations and strategies for their mitigation. *ACS Sensors* 2020;5:3306–27. <http://dx.doi.org/10.1021/acssensors.0c02019>.
- [26] Bannenberg L, Schreuders H, Dam B. Tantalum-palladium: Hysteresis-free optical hydrogen sensor over 7 orders of magnitude in pressure with sub-second response. *Adv Funct Mater* 2021;31. <http://dx.doi.org/10.1002/adfm.202010483>.
- [27] Bannenberg LJ, Blom L, Sakaki K, Asano K, Schreuders H. Completely elastic deformation of hydrogenated Ta thin films. *ACS Mater Lett* 2023;5:962–9. <http://dx.doi.org/10.1021/acsmaterialslett.3c00038>.
- [28] Bannenberg LJ, Schreuders H, van Beugen N, Kinane C, Hall S, Dam B. Tuning the properties of thin-film TaRu for hydrogen-sensing applications. *ACS Appl Mater Interfaces* 2023;15:8033–45. <http://dx.doi.org/10.1021/acsami.2c20112>.
- [29] Poate JM, Turner PA, Debonte WJ, Yahalom J. Thin-film interdiffusion. I. Au-Pd, Pd-Au, Ti-Pd, Ti-Au, Ti-Pd-Au, and Ti-Au-Pd. *J Appl Phys* 1975;46:4275–83. <http://dx.doi.org/10.1063/1.321411>.
- [30] Pacanowski S, Wachowiak M, Jabłoński B, Szymański B, Smardz L. Interface mixing and hydrogen absorption in Pd/Mg and Pd/Al/Mg thin films. *Int J Hydrog Energy* 2021;46(1):806–13. <http://dx.doi.org/10.1016/j.ijhydene.2020.09.175>.
- [31] Pivak Y, Schreuders H, Slaman M, Griessen R, Dam B. Thermodynamics, stress release and hysteresis behavior in highly adhesive Pd-H films. *Int J Hydrog Energy* 2011;36(6):4056–67. <http://dx.doi.org/10.1016/j.ijhydene.2010.12.063>, 3rd International Workshop in Hydrogen Energy.
- [32] Lee E, Lee JM, Koo JH, Lee W, Lee T. Hysteresis behavior of electrical resistance in Pd thin films during the process of absorption and desorption of hydrogen gas. *Int J Hydrog Energy* 2010;35(13):6984–91. <http://dx.doi.org/10.1016/j.ijhydene.2010.04.051>, ISMF-09.
- [33] Bannenberg LJ, Boshuizen B, Nugroho FAA, Schreuders H. Hydrogenation kinetics of metal hydride catalytic layers. *ACS Appl Mater Interfaces* 2021;13:52530–41. <http://dx.doi.org/10.1021/acsami.1c13240>.
- [34] Gremaud R, Broedersz CP, Borsa DM, Borgschulte A, Mauron P, Schreuders H, Rector JH, Dam B, Griessen R. Hydrogenography: An optical combinatorial method to find new light-weight hydrogen-storage materials. *Adv Mater* 2007;19:2813–7. <http://dx.doi.org/10.1002/adma.200602560>.
- [35] Björck M, Andersson G. GenX: an extensible X-ray reflectivity refinement program utilizing differential evolution. *J Appl Crystallogr* 2007;40(6):1174–8. <http://dx.doi.org/10.1107/S0021889807045086>.
- [36] Hu X, Xie Q, Zhang J, Yu Q, Liu H, Sun Y. Experimental study of the lower flammability limits of H<sub>2</sub>/O<sub>2</sub>/CO<sub>2</sub> mixture. *Int J Hydrog Energy* 2020;45(51):27837–45. <http://dx.doi.org/10.1016/j.ijhydene.2020.07.033>, URL <https://www.sciencedirect.com/science/article/pii/S0360319920325659>.
- [37] Keçebaş A, Kayfeci M. Chapter 1 - hydrogen properties. In: Calise F, D'Accadia MD, Santarelli M, Lanzini A, Ferrero D, editors. *Solar hydrogen production*. Academic Press; 2019, p. 3–29. <http://dx.doi.org/10.1016/B978-0-12-814853-2.00001-1>, URL <https://www.sciencedirect.com/science/article/pii/B9780128148532000011>.
- [38] Eltherington J. *Standard test method for linear thermal expansion of solid materials with a vitreous silica dilatometer*. 1998.
- [39] Fang W, Lo C-Y. On the thermal expansion coefficients of thin films. *Sensors Actuators A* 2000;84(3):310–4. [http://dx.doi.org/10.1016/S0924-4247\(00\)00311-3](http://dx.doi.org/10.1016/S0924-4247(00)00311-3).